41st ISYA Lecturer: *Gustavo Bruzual, IRyA, UNAM; Campus Morelia, México*

Topic: *GALAXIES (6 lectures)*

Description: An overview of the basic properties of galaxies due to the distribution, kinematics, dynamics, relevance, and evolution of their different stellar populations. A view of the basic properties and processes in the distant universe as revealed by galaxies of all types discovered so far.

Syllabus:

Lecture 1: **The Milky Way as a galaxy**
- The structure of the Galaxy
- The galactic disk
- The galactic bulge
- The galactic halo
- The galactic center
- Velocity of the sun
- Rotation curve of the Galaxy
- Stellar populations in the Galaxy

Lecture 2: **The world of galaxies (1)**
- Morphological classification. The Hubble Sequence
- Other types of galaxies
- Elliptical galaxies
- Spiral galaxies
- Galaxies in the local group
- Scaling relations

Lecture 3: **The world of galaxies (2)**
- The extragalactic distance scale
- The luminosity function of galaxies
- Black holes in the centers of galaxies
- Galaxies as gravitational lenses
- Stellar population synthesis
- Spectral evolution of galaxies
- Chemical evolution of galaxies

Lecture 4: **Clusters and groups of galaxies**
- The local group
- Galaxies in clusters and groups
- Morphological classification of clusters
- Spatial distribution of galaxies in clusters
- Luminosity function of cluster galaxies
- Clusters of galaxies as gravitational lenses
- Evolution of clusters

Lecture 5: **Galaxies at high redshift (1)**
- Lyman-break galaxies
- Starburst galaxies
- Extremely red objects
- Sub-millimeter sources
- Damped Lyman-alpha systems
- Lyman-alpha blobs
- Gamma-ray bursts

Lecture 6: **Galaxies at high redshift (2)**
- Background radiation
- Re-ionization of the universe
- Cosmic star formation history
- Galaxy formation and evolution

Requirements: Video projector in the class room

Bibliography:

- Schneider, *Extragalactic astronomy and cosmology*
- Sparke & Gallager, *Galaxies in the Universe*
- Mo, van den Bosch & White, Galaxy formation and evolution (selected chapters)

The World of Galaxies (1)

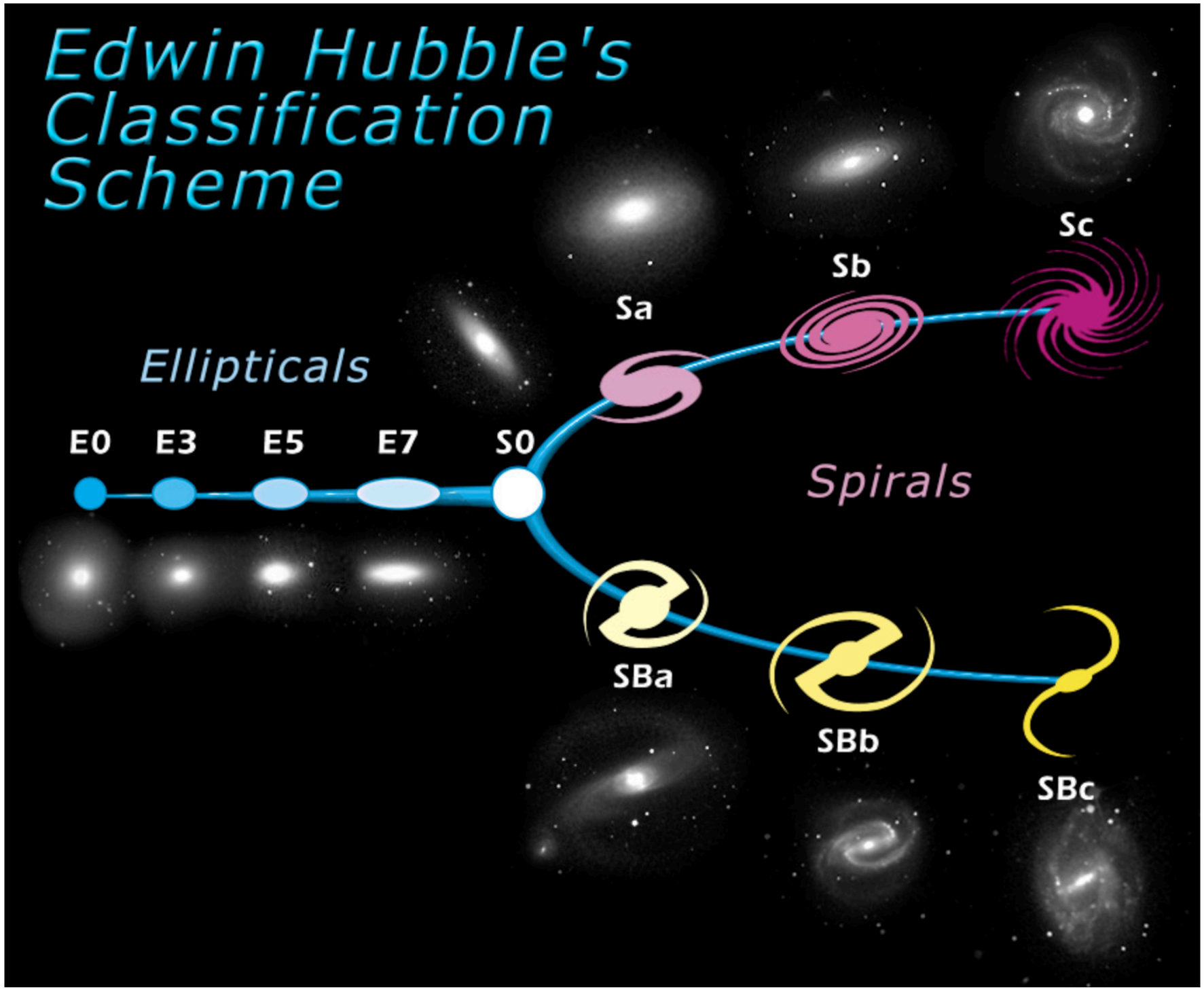


Elliptical Galaxy ESO 325-G004 in the Abell Cluster S0740
Hubble Heritage
NASA, ESA, and The Hubble Heritage Team (STScI/AURA) • HST/ACS • STScI-PRC07-08

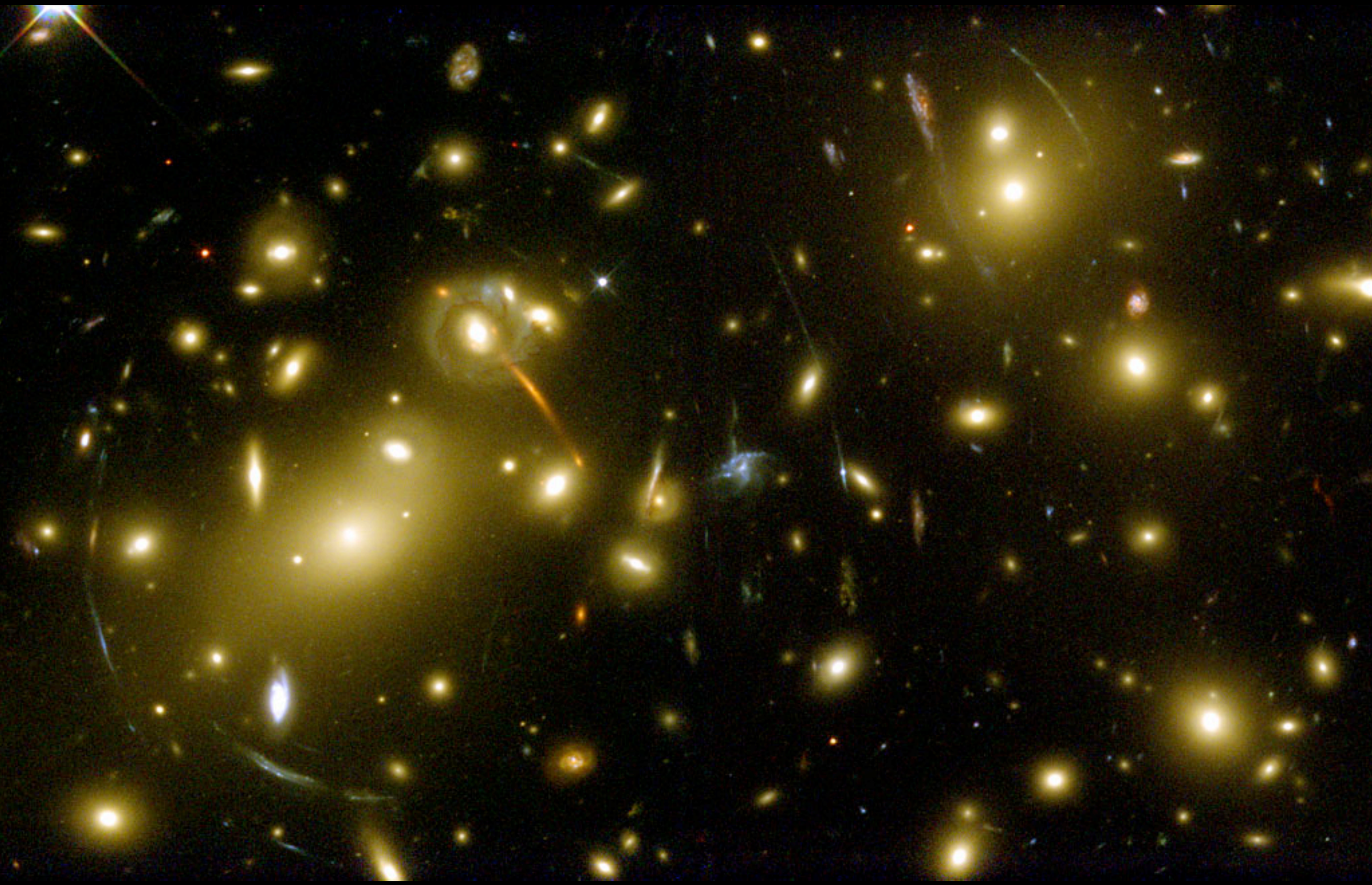

Distant Gravitationally Lensed Galaxy
Galaxy Cluster Abell 1689

Hubble Space Telescope
ACS/WFC NICMOS

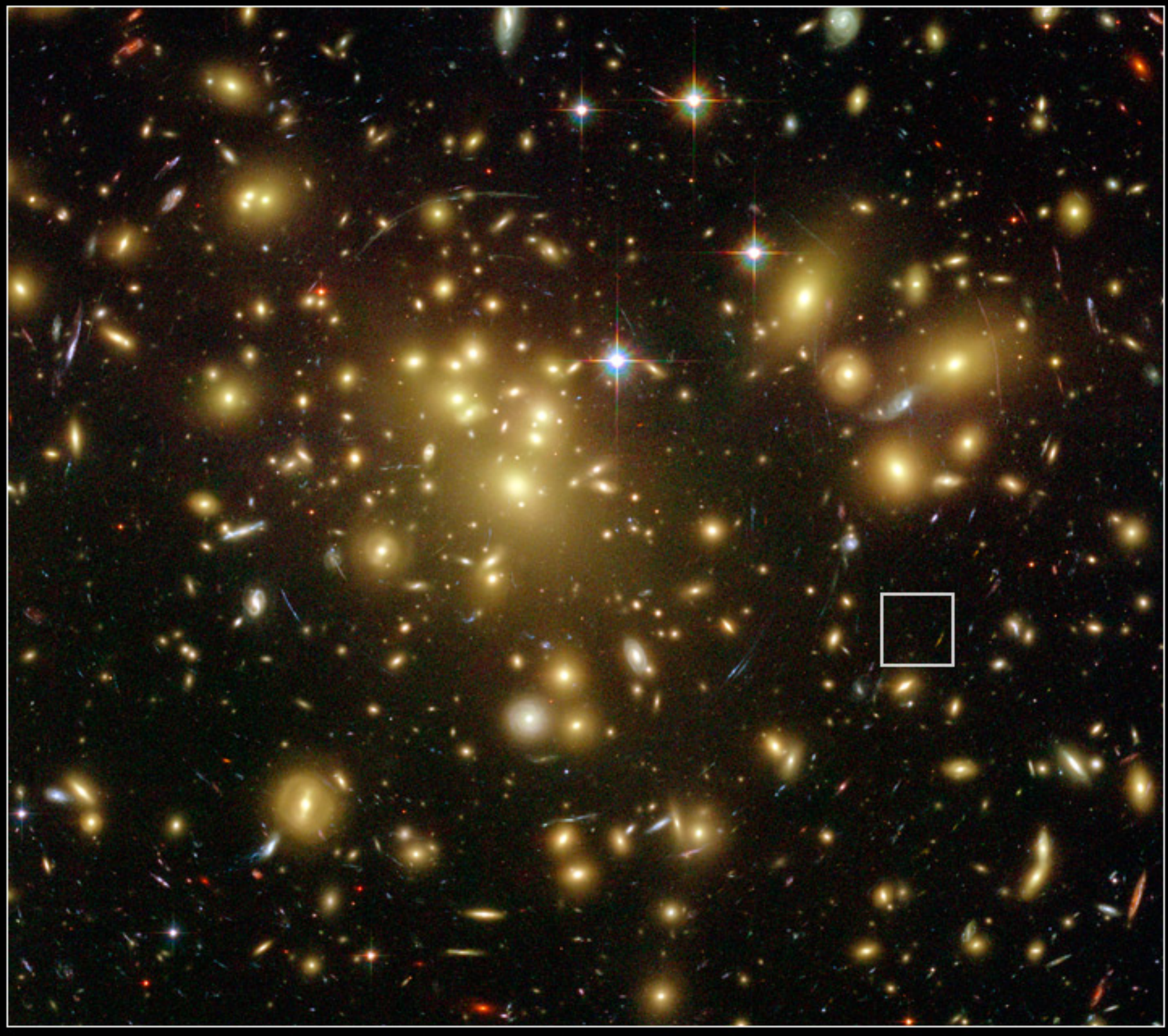

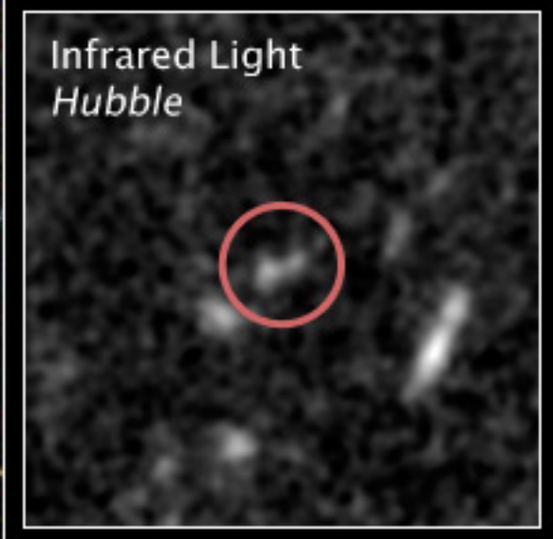

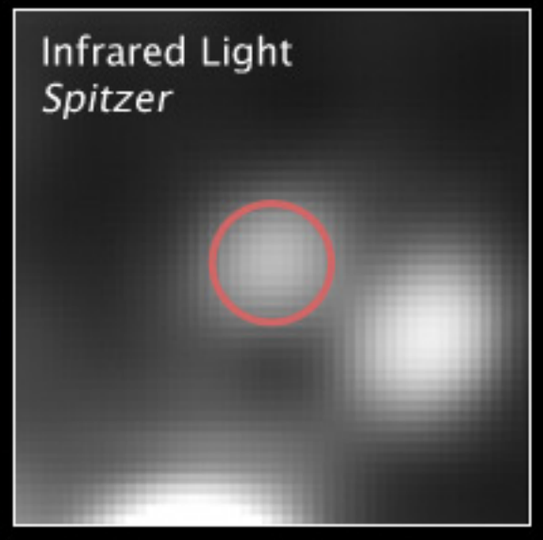

NASA, ESA, and L. Bradley (JHU), R. Bouwens (UCSC), H. Ford (JHU), and G. Illingworth (UCSC)

STScI-PRC08-08a

HDF

Hubble Deep Field

ST ScI OPO January 15, 1996 R. WIlliams and the HDF Team (ST ScI) and NASA

HST WFPC2

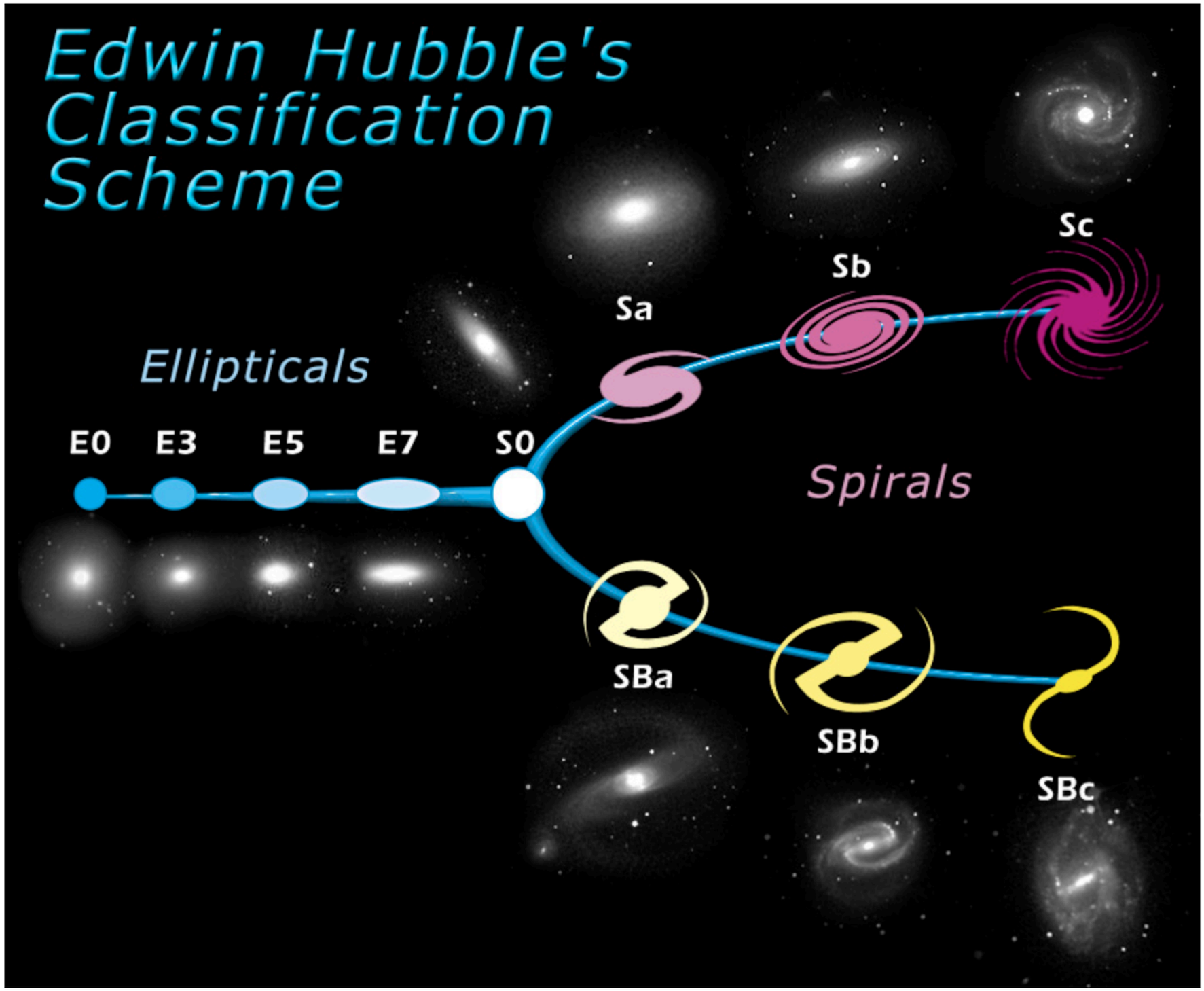
Edwin Hubble's Classification Scheme
Ellipticals
E0
E3
E5
E7
S0
Sa
Sb
Sc
Spirals
SBa
SBb
SBc

Morphological Classification (The Hubble sequence)

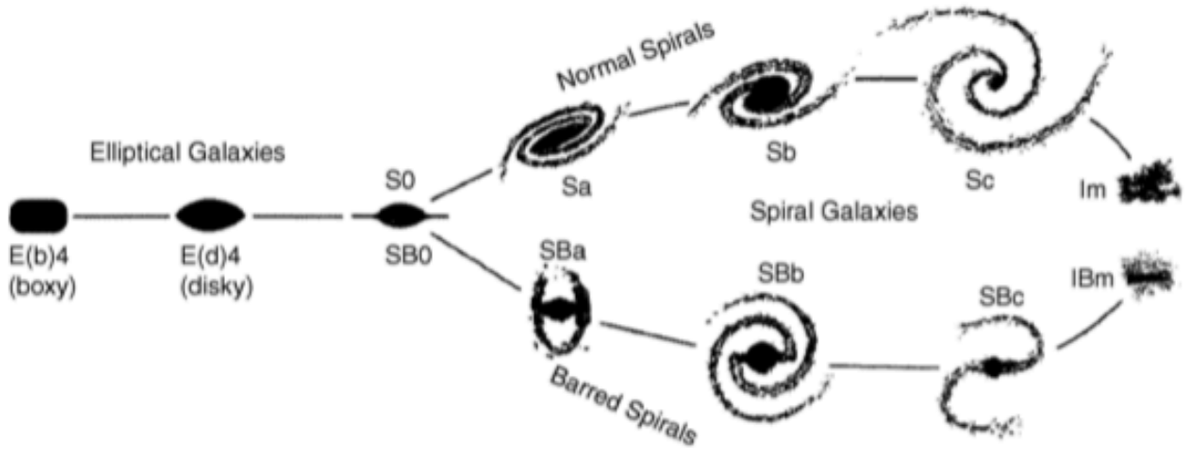

Fig. 3.2. Hubble's "tuning fork" for galaxy classification

Obviously, the morphological classification is at least partially affected by projection effects. If, for instance, the spatial shape of an elliptical galaxy is a triaxial ellipsoid, then the observed ellipticity ϵ will depend on its orientation with respect to the line-of-sight. Also, it will be difficult to identify a bar in a spiral that is observed from its side ("edge-on").

- *Elliptical galaxies* (E's) are galaxies that have nearly elliptical isophotes[1] without any clearly defined structure. They are subdivided according to their ellipticity $\epsilon \equiv 1 - b/a$, where a and b denote the semimajor and the semiminor axes, respectively. Ellipticals are found over a relatively broad range in ellipticity, $0 \leq \epsilon \lesssim 0.7$. The notation E$n$ is commonly used to classify the ellipticals with respect to ϵ, with $n = 10\epsilon$; i.e., an E4 galaxy has an axis ratio of $b/a = 0.6$, and E0's have circular isophotes.

- *S0 galaxies* are a transition between ellipticals and spirals. They are also called lenticulars as they are lentil-shaped galaxies which are likewise subdivided into S0 and SB0, depending on whether or not they show a bar. They contain a bulge and a large enveloping region of relatively unstructured brightness which often appears like a disk without spiral arms. Ellipticals and S0 galaxies are referred to as early-type galaxies, spirals as late-type galaxies. As before, these names are only historical and are not meant to describe an evolutionary track!

- *Spiral galaxies* consist of a disk with spiral arm structure and a central bulge. They are divided into two subclasses: *normal spirals* (S's) and *barred spirals* (SB's). In each of these subclasses, a sequence is defined that is ordered according to the brightness ratio of bulge and disk, and that is denoted by a, ab, b, bc, c, cd, d. Objects along this sequence are often referred to as being either an early-type or a late-type; hence, an Sa galaxy is an early-type spiral, and an SBc galaxy is a late-type barred spiral. We stress explicitly that this nomenclature is not a statement of the evolutionary stage of the objects but is merely a nomenclature of purely historical origin.

- *Irregular galaxies* (Irr's) are galaxies with only weak (Irr I) or no (Irr II) regular structure. The classification of Irr's is often refined. In particular, the sequence of spirals is extended to the classes Sdm, Sm, Im, and Ir (m stands for Magellanic; the Large Magellanic Cloud is of type SBm).

3.2 Elliptical Galaxies

3.2.1 Classification

The general term "elliptical galaxies" (or ellipticals, for short) covers a broad class of galaxies which differ in their luminosities and sizes – some of them are displayed in Fig. 3.5. A rough subdivision is as follows:

- *Normal ellipticals*. This class includes giant ellipticals (gE's), those of intermediate luminosity (E's), and compact ellipticals (cE's), covering a range in absolute magnitudes from $M_B \sim -23$ to $M_B \sim -15$. In addition, S0 galaxies are often assigned to this class of early-type galaxies.
- *Dwarf ellipticals* (dE's). These differ from the cE's in that they have a significantly smaller surface brightness and a lower metallicity.
- *cD galaxies*. These are extremely luminous (up to $M_B \sim -25$) and large (up to $R \lesssim 1$ Mpc) galaxies that are only found near the centers of dense clusters of galaxies. Their surface brightness is very high close to the center, they have an extended diffuse envelope, and they have a very high M/L ratio.
- *Blue compact dwarf galaxies.* These "blue compact dwarfs" (BCD's) are clearly bluer (with $\langle B-V \rangle$ between 0.0 and 0.3) than the other ellipticals, and contain an appreciable amount of gas in comparison.
- *Dwarf spheroidals* (dSph's) exhibit a very low luminosity and surface brightness. They have been observed down to $M_B \sim -8$. Due to these properties, they have thus far only been observed in the Local Group.

Thus elliptical galaxies span an enormous range (more than 10^6) in luminosity and mass, as is shown by the compilation in Table 3.1.

Table 3.1. Characteristic values for elliptical galaxies. D_{25} denotes the diameter at which the surface brightness has decreased to 25 B-mag/arcsec^2, S_N is the "specific frequency", a measure for the number of globular clusters in relation to the visual luminosity (see (3.13)), and M/L is the mass-to-light ratio in Solar units (the values of this table are taken from the book by Carroll & Ostlie, 1996)

	S0	cD	E	dE	dSph	BCD
M_B	-17 to -22	-22 to -25	-15 to -23	-13 to -19	-8 to -15	-14 to -17
$M(M_\odot)$	10^{10} to 10^{12}	10^{13} to 10^{14}	10^8 to 10^{13}	10^7 to 10^9	10^7 to 10^8	$\sim 10^9$
D_{25} (kpc)	10–100	300–1000	1–200	1–10	0.1–0.5	< 3
$\langle M/L_B \rangle$	~ 10	> 100	10–100	1–10	5–100	0.1–10
$\langle S_N \rangle$	~ 5	~ 15	~ 5	4.8 ± 1.0	–	–

3.2.2 Brightness Profile

The brightness profiles of normal E's and cD's follow a de Vaucouleurs profile (see (2.39) or (2.41), respectively) over a wide range in radius, as is demonstrated in Fig. 3.6. The effective radius R_e is strongly correlated with the absolute magnitude M_B, as can be seen in Fig. 3.7, with rather little scatter. In comparison, the dE's and the dSph's clearly follow a different distribution. Owing to the relation (2.42) between luminosity, effective radius and central surface brightness, an analogous relation exists for the average surface brightness μ_{ave} (unit: $B-mag/arcsec^2$) within R_e as a function of M_B. In particular, the surface brightness in normal E's decreases with increasing luminosity, while it increases for dE's and dSph's.

Yet another way of expressing this correlation is by eliminating the absolute luminosity, thus obtaining a relation between effective radius R_e and surface brightness μ_{ave}. This form is then called the Kormendy relation.

The de Vaucouleurs profile provides the best fits for normal E's, whereas for E's with exceptionally high (or low) luminosity the profile decreases more slowly (or rapidly) for larger radii. The profile of cD's extends much farther out and is not properly described by a de Vaucouleurs profile (Fig. 3.8), except in its innermost part. It appears that cD's are similar to E's but embedded in a very extended, luminous halo. Since cD's are only found in the centers of massive clusters of galaxies, a connection must exist between this morphology and the environment of these galaxies. In contrast to these classes of ellipticals, diffuse dE's are often better described by an exponential profile.

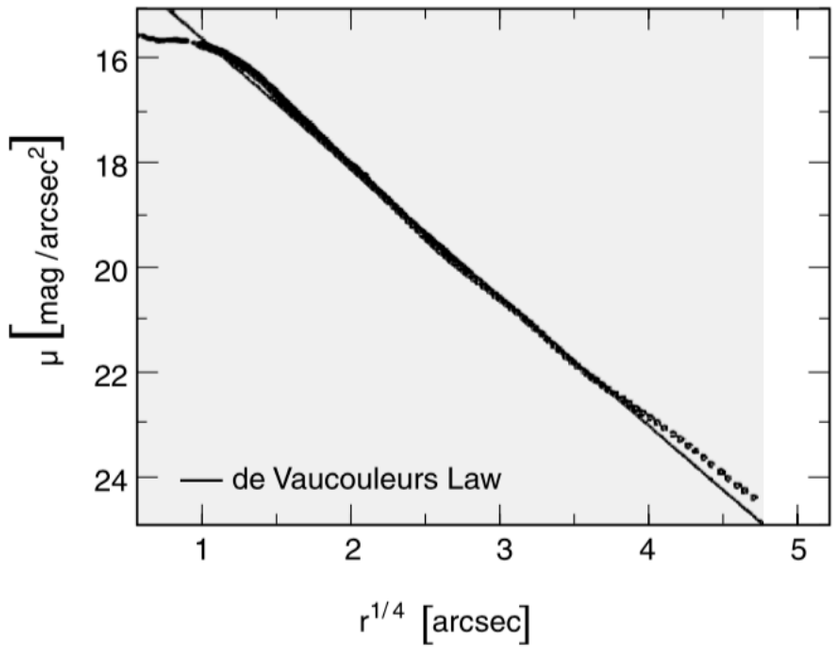

Fig. 3.6. Surface brightness profile of the galaxy NGC 4472, fitted by a de Vaucouleurs profile. The de Vaucouleurs profile describes a linear relation between the logarithm of the intensity (i.e., linear on a magnitude scale) and $r^{1/4}$; for this reason, it is also called an $r^{1/4}$-law

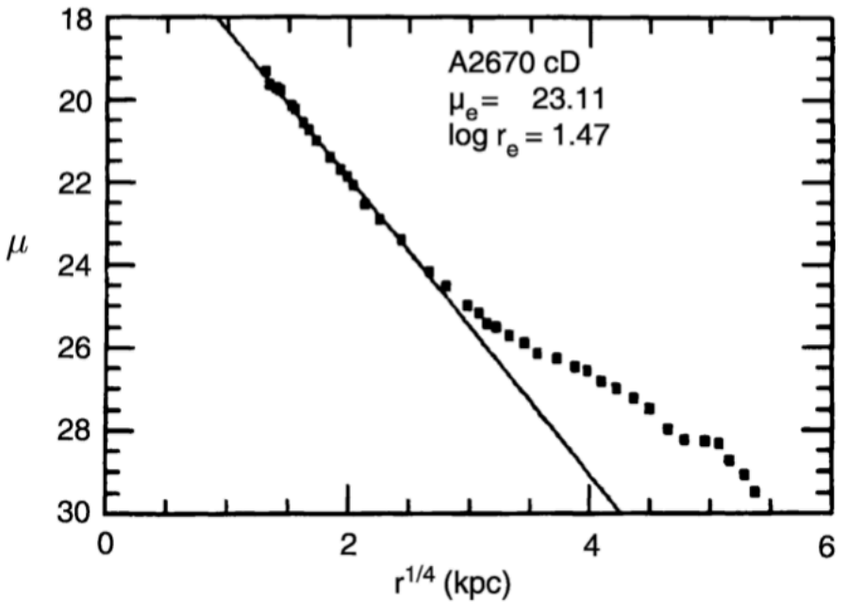

Fig. 3.8. Comparison of the brightness profile of a cD galaxy, the central galaxy of the cluster of galaxies Abell 2670, with a de Vaucouleurs profile. The light excess for large radii is clearly visible

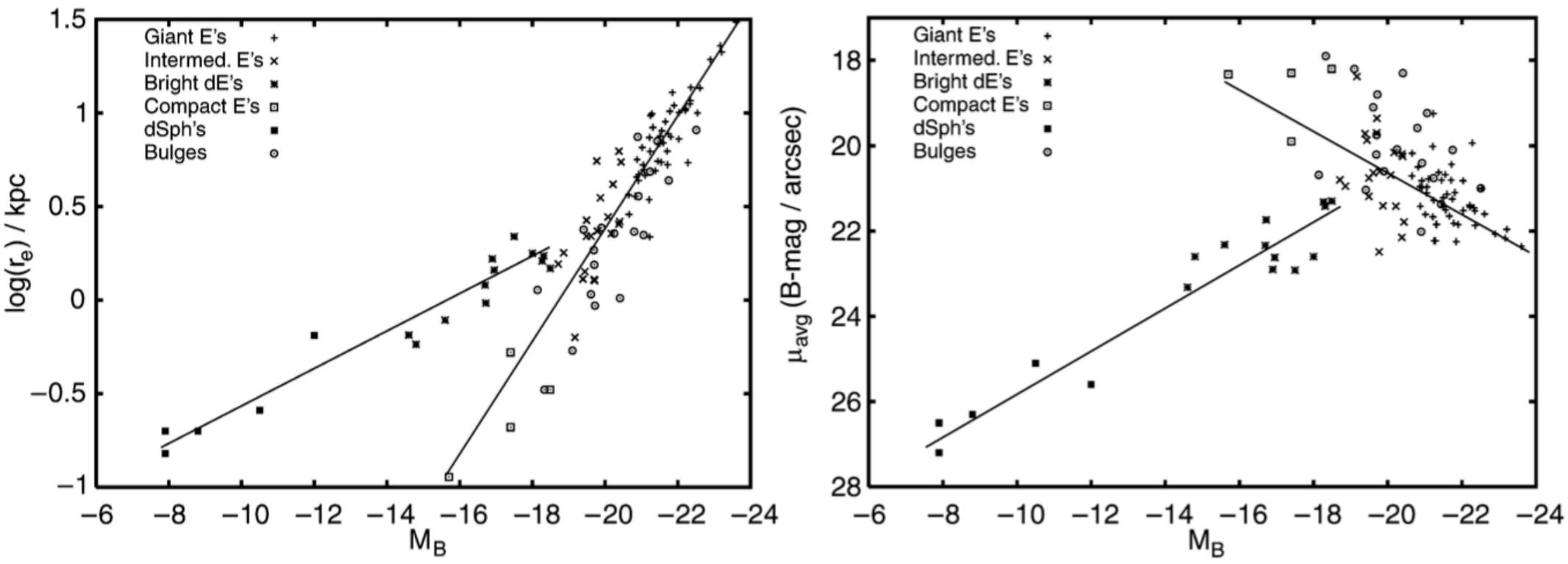

Fig. 3.7. Left panel: effective radius R_e versus absolute magnitude M_B; the correlation for normal ellipticals is different from that of dwarfs. Right panel: average surface brightness μ_{ave} versus M_B; for normal ellipticals, the surface brightness decreases with increasing luminosity while for dwarfs it increases

3.2.4 Dynamics of Elliptical Galaxies

Analyzing the morphology of elliptical galaxies raises a simple question: *Why are ellipticals not round?* A simple explanation would be rotational flattening, i.e., as in a rotating self-gravitating gas ball, the stellar distribution bulges outwards at the equator due to centrifugal forces, as is also the case for the Earth. If this explanation were correct, the rotational velocity v_{rot}, which is measurable in the relative Doppler shift of absorption lines, would have to be of about the same magnitude as the velocity dispersion of the stars σ_v that is measurable through the Doppler broadening of lines. More precisely, by means of stellar dynamics one can show that for the rotational flattening of an axially symmetric, oblate[2] galaxy, the relation

$$\left(\frac{v_{\mathrm{rot}}}{\sigma_v}\right)_{\mathrm{iso}} \approx \sqrt{\frac{\epsilon}{1-\epsilon}} \tag{3.1}$$

has to be satisfied, where "iso" indicates the assumption of an isotropic velocity distribution of the stars. However, for luminous ellipticals one finds that, in general, $v_{\mathrm{rot}} \ll \sigma_v$, so that rotation cannot be the major cause of their ellipticity (see Fig. 3.9). In addition, many ellipticals are presumably triaxial, so that no unambiguous rotation axis is defined. Thus, luminous ellipticals are in general *not* rotationally flattened. For less luminous ellipticals and for the bulges of disk galaxies, however, rotational flattening can play an important role. The question remains of how to explain a stable elliptical distribution of stars without rotation.

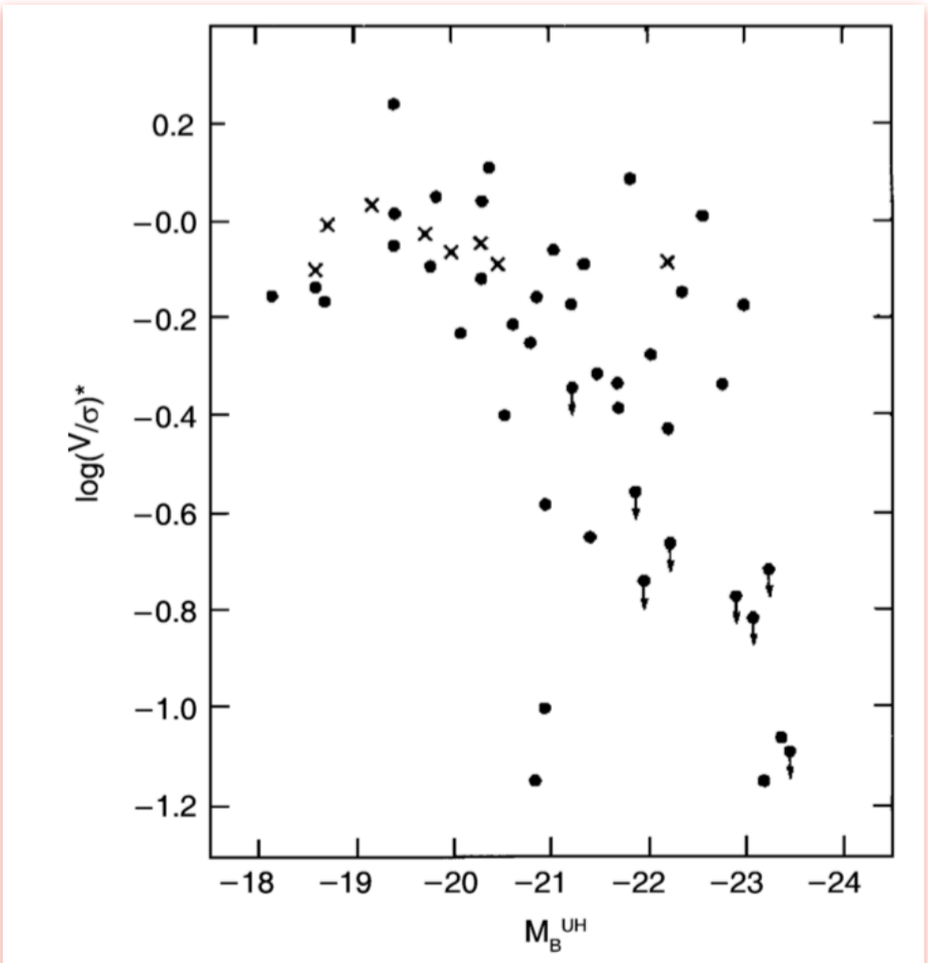

Fig. 3.9. The rotation parameter $\left(\frac{v_{\mathrm{rot}}}{\sigma_v}\right) / \left(\frac{v_{\mathrm{rot}}}{\sigma_v}\right)_{\mathrm{iso}}$ of elliptical galaxies, here denoted by $(\mathrm{V}/\sigma)^*$, plotted as a function of absolute magnitude. Dots denote elliptical galaxies, crosses the bulges of disk galaxies

Relaxation Time-Scale. The question now arises whether such an equilibrium system can also be stable in time. One might expect that close encounters of pairs of stars would cause a noticeable disturbance in the distribution of orbits. These pair-wise collisions could then lead to a "thermalization" of the stellar orbits.[3] To examine this question we need to estimate the time-scale for such collisions and the changes in direction they cause.

For this purpose, we consider the relaxation time-scale by pair collisions in a system of N stars of mass m, total mass $M = Nm$, extent R, and a mean stellar density of $n = 3N/(4\pi R^3)$. We define the relaxation time $t_{\rm relax}$ as the characteristic time in which a star changes its velocity direction by $\sim 90°$ due to pair collisions with other stars. By simple calculation (see below), we find that

$$t_{\rm relax} \approx \frac{R}{v}\frac{N}{\ln N}\,, \qquad (3.2)$$

or

$$\boxed{t_{\rm relax} = t_{\rm cross}\frac{N}{\ln N}}\,, \qquad (3.3)$$

where $t_{\rm cross} = R/v$ is the crossing time-scale, i.e., the time it takes a star to cross the stellar system. If we now consider a typical galaxy, with $t_{\rm cross} \sim 10^8$ yr, $N \sim 10^{12}$ (thus $\ln N \sim 30$), then we find that the relaxation time is much longer than the age of the Universe. This means that *pair collisions do not play any role in the evolution of stellar orbits*. The dynamics of the orbits are determined solely by the large-scale gravitational field of the galaxy. In Sect. 7.5.1, we will describe a process called violent relaxation which most likely plays a central role in the formation of galaxies and which is probably also responsible for the stellar orbits establishing an equilibrium configuration.

The stars behave like a collisionless gas: elliptical galaxies are stabilized by (dynamical) pressure, and they are elliptical because the stellar distribution is anisotropic in velocity space. This corresponds to an anisotropic pressure – where we recall that the pressure of a gas is nothing but the momentum transport of gas particles due to their thermal motions.

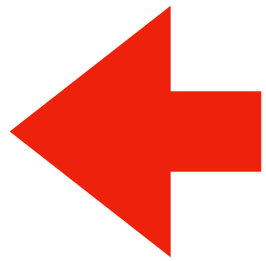

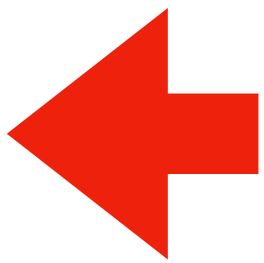

Boxiness and Diskiness. The so-called boxiness parameter describes the deviation of the isophotes' shape from that of an ellipse. Consider the shape of an isophote. If it is described by an ellipse, then after a suitable choice of the coordinate system, $\theta_1 = a\cos t$, $\theta_2 = b\sin t$, where a and b are the two semi-axes of the ellipse and $t \in [0, 2\pi]$ parametrizes the curve. The distance $r(t)$ of a point from the center is

$$r(t) = \sqrt{\theta_1^2 + \theta_2^2} = \sqrt{\frac{a^2+b^2}{2} + \frac{a^2-b^2}{2}\cos(2t)}\ .$$

Deviations of the isophote shape from this ellipse are now expanded in a Taylor series, where the term $\propto \cos(4t)$ describes the lowest-order correction that preserves the symmetry of the ellipse with respect to reflection in the two coordinate axes. The modified curve is then described by

$$\boldsymbol{\theta}(t) = \left(1 + \frac{a_4\ \cos(4t)}{r(t)}\right)\begin{pmatrix} a\cos t \\ b\sin t \end{pmatrix}\ , \qquad (3.9)$$

with $r(t)$ as defined above. The parameter a_4 thus describes a deviation from an ellipse: if $a_4 > 0$, the isophote appears more disk-like, and if $a_4 < 0$, it becomes rather boxy (see Fig. 3.11). In elliptical galaxies we typically find $|a_4/a| \sim 0.01$, thus only a small deviation from the elliptical form.

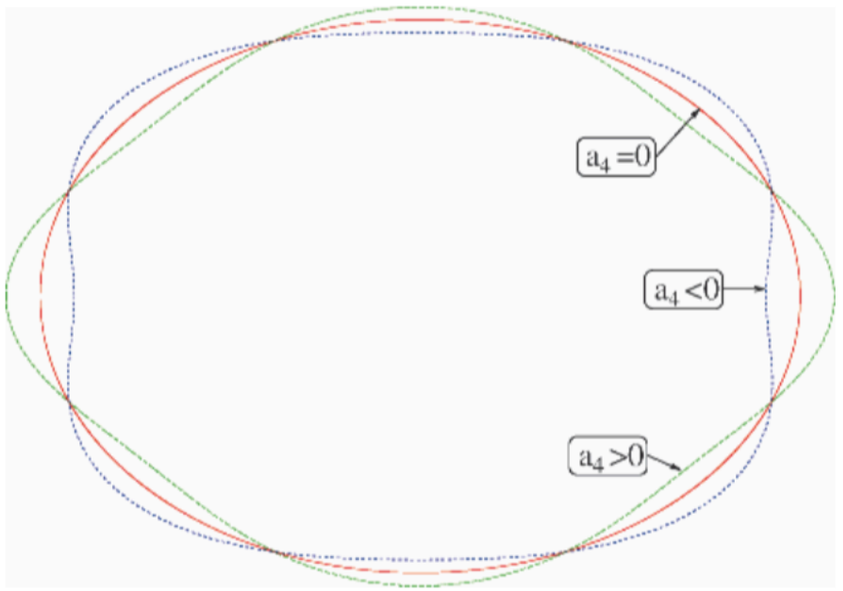

Fig. 3.11. Sketch to illustrate boxiness and diskiness. The solid red curve shows an ellipse ($a_4 = 0$), the green dashed curve a disky ellipse ($a_4 > 0$), and the blue dotted curve a boxy ellipse ($a_4 < 0$). In elliptical galaxies, the deviations in the shape of the isophotes from an ellipse are considerably smaller than in this sketch

Correlations of a_4 with Other Properties of Ellipticals. Surprisingly, we find that the parameter a_4/a is strongly correlated with other properties of ellipticals (see Fig. 3.12). The ratio $\left(\frac{v_{\rm rot}}{\sigma_v}\right) \Big/ \left(\frac{v_{\rm rot}}{\sigma_v}\right)_{\rm iso}$ (upper left in Fig. 3.12) is of order unity for disky ellipses ($a_4 > 0$) and, in general, significantly smaller than 1 for boxy ellipticals. From this we conclude that "diskies" are in part rotationally supported, whereas the flattening of "boxies" is mainly caused by the anisotropic distribution of their stellar orbits in velocity space. The mass-to-light ratio is also correlated with a_4: boxies (diskies) have a value of M/L in their core which is larger (smaller) than the mean elliptical of comparable luminosity. A very strong correlation exists between a_4/a and the radio luminosity of ellipticals: while diskies are weak radio emitters, boxies show a broad distribution in $L_{\rm radio}$. These correlations are also seen in the X-ray luminosity, since diskies are weak X-ray emitters and boxies have a broad distribution in $L_{\rm X}$. This bimodality becomes even more obvious if the radiation contributed by compact sources (e.g., X-ray binary stars) is subtracted from the total X-ray luminosity, thus considering only the diffuse X-ray emission. Ellipticals with a different sign of a_4 also differ in the kinematics of their stars: boxies often have cores spinning against the general direction of rotation (counter-rotating cores), which is rarely observed in diskies.

About 70% of the ellipticals are diskies. The transition between diskies and S0 galaxies may be continuous along a sequence of varying disk-to-bulge ratio.

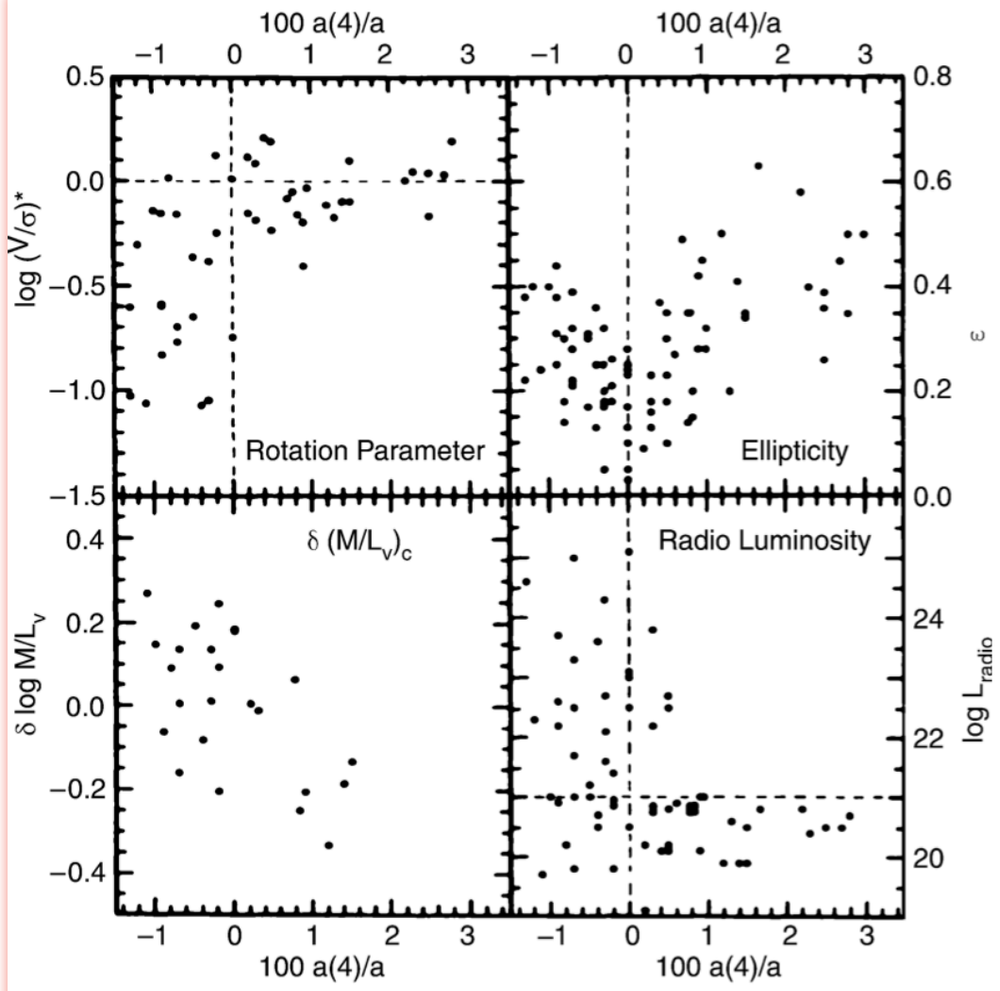

Fig. 3.12. Correlations of a_4/a with some other properties of elliptical galaxies. $100a(4)/a$ (corresponding to a_4/a) describes the deviation of the isophote shape from an ellipse in percent. Negative values denote boxy ellipticals, positive values disky ellipticals. The upper left panel shows the rotation parameter discussed in Sect. 3.2.4; at the lower left, the deviation from the average mass-to-light ratio is shown. The upper right panel shows the ellipticity, and the lower right panel displays the radio luminosity at 1.4 GHz. Obviously, there is a correlation of all these parameters with the boxiness parameter

Shells and Ripples. In about 40% of the early-type galaxies that are not member galaxies of a cluster, sharp discontinuities in the surface brightness are found, a kind of shell structure ("shells" or "ripples"). They are visible as elliptical arcs curving around the center of the galaxy (see Fig. 3.13). Such sharp edges can only be formed if the corresponding distribution of stars is "cold", i.e., they must have a very small velocity dispersion, since otherwise such coherent structures would smear out on a very short time-scale. As a comparison, we can consider disk galaxies that likewise contain sharp structures, namely the thin stellar disk. Indeed, the stars in the disk have a very small velocity dispersion, ~ 20 km/s, compared to the rotational velocity of typically 200 km/s.

These peculiarities in ellipticals are not uncommon. Indicators for shells can be found in about half of the early-type galaxies, and about a third of them show boxy isophotes.

> Boxiness, counter-rotating cores, and shells and ripples are all indicators of a complex evolution that is probably caused by past mergers with other galaxies.

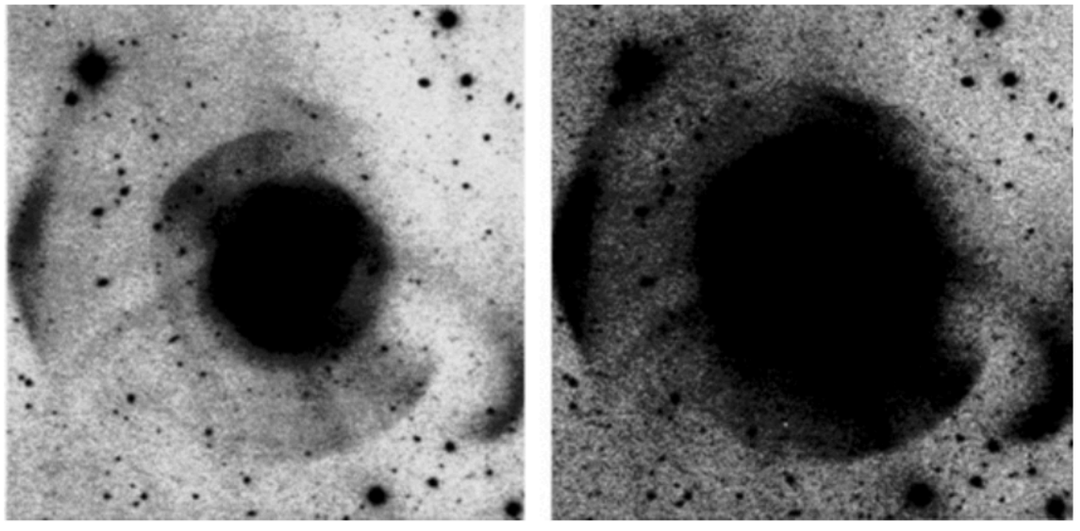

Fig. 3.13. In the galaxy NGC 474, here shown in two images of different contrast, a number of sharp-edged elliptical arcs are visible around the center of the galaxy, the so-called ripples or shells. The displayed image corresponds to a linear scale of about 90 kpc

3.3 Spiral Galaxies

3.3.1 Trends in the Sequence of Spirals

Looking at the sequence of early-type spirals (i.e., Sa's or SBa's) to late-type spirals, we find a number of differences that can be used for classification (see also Fig. 3.14):

- a decreasing luminosity ratio of bulge and disk, with $L_{\rm bulge}/L_{\rm disk} \sim 0.3$ for Sa's and ~ 0.05 for Sc's;
- an increasing opening angle of the spiral arms, from $\sim 6°$ for Sa's to $\sim 18°$ for Sc's;
- and an increasing brightness structure along the spiral arms: Sa's have a "smooth" distribution of stars along the spiral arms, whereas the light distribution in the spiral arms of Sc's is resolved into bright knots of stars and HII regions.

Compared to ellipticals, the spirals cover a distinctly smaller range in absolute magnitude (and mass). They are limited to $-16 \gtrsim M_B \gtrsim -23$ and $10^9 M_\odot \lesssim M \lesssim 10^{12} M_\odot$, respectively. Characteristic parameters of the various types of spirals are compiled in Table 3.2.

Bars are common in spiral galaxies, with $\sim 70\%$ of all disk galaxies containing a large-scale stellar bar. Such a bar perturbs the axial symmetry of the gravitational potential in a galaxy, which may have a number of consequences. One of them is that this perturbation can lead to a redistribution of angular momentum of the stars, gas, and dark matter. In addition, by perturbing the orbits, gas can be driven towards the center of the galaxy which may have important consequences for triggering nuclear activity (see Chap. 5).

Table 3.2. Characteristic values for spiral galaxies. $V_{\rm max}$ is the maximum rotation velocity, thus characterizing the flat part of the rotation curve. The opening angle is the angle under which the spiral arms branch off, i.e., the angle between the tangent to the spiral arms and the circle around the center of the galaxy running through this tangential point. $S_{\rm N}$ is the specific abundance of globular clusters as defined in (3.13). The values in this table are taken from the book by Carroll & Ostlie (1996)

	Sa	Sb	Sc	Sd/Sm	Im/Ir
M_B	−17 to −23	−17 to −23	−16 to −22	−15 to −20	−13 to −18
$M\,(M_\odot)$	10^9–10^{12}	10^9–10^{12}	10^9–10^{12}	10^8–10^{10}	10^8–10^{10}
$\langle L_{\rm bulge}/L_{\rm tot}\rangle_B$	0.3	0.13	0.05	–	–
Diam. (D_{25}, kpc)	5–100	5–100	5–100	0.5–50	0.5–50
$\langle M/L_{\rm B}\rangle\,(M_\odot/L_\odot)$	6.2 ± 0.6	4.5 ± 0.4	2.6 ± 0.2	~ 1	~ 1
$\langle V_{\rm max}\rangle$(km s^{-1})	299	222	175	–	–
$V_{\rm max}$ range (km s^{-1})	163–367	144–330	99–304	–	50–70
Opening angle	$\sim 6°$	$\sim 12°$	$\sim 18°$	–	–
$\mu_{0,\rm B}$ (mag arcsec^{-2})	21.52 ± 0.39	21.52 ± 0.39	21.52 ± 0.39	22.61 ± 0.47	22.61 ± 0.47
$\langle B-V\rangle$	0.75	0.64	0.52	0.47	0.37
$\langle M_{\rm gas}/M_{\rm tot}\rangle$	0.04	0.08	0.16	0.25 (Scd)	–
$\langle M_{\rm H_2}/M_{\rm HI}\rangle$	2.2 ± 0.6 (Sab)	1.8 ± 0.3	0.73 ± 0.13	0.19 ± 0.10	–
$\langle S_{\rm N}\rangle$	1.2 ± 0.2	1.2 ± 0.2	0.5 ± 0.2	0.5 ± 0.2	–

3.3.2 Brightness Profile

The light profile of the bulge of spirals is described by a de Vaucouleurs profile to a good approximation – see (2.39) and (2.41) – while the disk follows an exponential brightness profile, as is the case for our Milky Way. Expressing these distributions of the surface brightness in $\mu \propto -2.5 \log(I)$, measured in mag/arcsec^2, we obtain

$$\mu_{\rm bulge}(R) = \mu_{\rm e} + 8.3268 \left[\left(\frac{R}{R_{\rm e}} \right)^{1/4} - 1 \right] \quad (3.10)$$

and

$$\mu_{\rm disk}(R) = \mu_0 + 1.09 \left(\frac{R}{h_r} \right) . \quad (3.11)$$

Here, $\mu_{\rm e}$ is the surface brightness at the effective radius $R_{\rm e}$ which is defined such that half of the luminosity is emitted within $R_{\rm e}$ (see (2.40)). The central surface brightness and the scale-length of the disk are denoted by μ_0 and h_r, respectively. It has to be noted that μ_0 is not directly measurable since μ_0 is *not* the central surface brightness of the galaxy, only that of its disk component. To determine μ_0, the exponential law (3.11) is extrapolated from large R inwards to $R = 0$.

Whereas the bulge and the disk can be studied in spirals even at fairly large distances, the stellar halo has too low a surface brightness to be seen in distant galaxies. However, our neighboring galaxy M31, the Andromeda galaxy, can be studied in quite some detail. In particular, the brightness profile of its stellar halo can be studied more easily than that of the Milky Way, taking advantage of our "outside" view. This galaxy should be quite similar to our Galaxy in many respects; for example, tidal streams from disrupted accreted galaxies were also clearly detected in M31.

Halo

A stellar halo of red giant branch stars was detected in M31, which extends out to more than 150 kpc from its center. The brightness profile of this stellar distribution indicates that for radii $r \lesssim 20$ kpc it follows the extrapolation from the brightness profile of the bulge, i.e., a de Vaucouleurs profile. However, for larger radii it exceeds this extrapolation, showing a power-law profile which corresponds to a radial density profile of approximately $\rho \propto r^{-3}$, not unlike that observed in our Milky Way. It thus seems that stellar halos form a generic property of spirals. Unfortunately, the corresponding surface brightness is so small that there is little hope of detecting such a halo in other spirals for which individual stars can no longer be resolved and classified.

Thick Disk

The thick disk in other spirals can only be studied if they are oriented edge-on. In these cases, a thick disk can indeed be observed as a stellar population outside the plane of the disk and well beyond the scale-height of the thin disk. As is the case for the Milky Way, the scale-height of a stellar population increases with its age, increasing from young main-sequence stars to old asymptotic giant branch stars. For luminous disk galaxies, the thick disk does not contribute substantially to the total luminosity; however, in lower-mass disk galaxies with rotational velocities $\lesssim 120$ km/s, the thick disk stars can contribute nearly half the luminosity and may actually dominate the stellar mass. In this case, the dominant stellar population of these galaxies is old, despite the fact that they appear blue.

3.3.3 Rotation Curves and Dark Matter

The rotation curves of other spiral galaxies are easier to measure than that of the Milky Way because we are able to observe them "from outside". These measurements are achieved by utilizing the Doppler effect, where the inclination of the disk, i.e., its orientation with respect to the line-of-sight, has to be accounted for. The inclination angle is determined from the observed axis ratio of the disk, assuming that disks are intrinsically axially symmetric (except for the spiral arms). Mainly the stars and HI gas in the galaxies are used as luminous tracers, where the observable HI disk is in general significantly more extended than the stellar disk. Therefore, the rotation curves measured from the 21-cm line typically extend to much larger radii than those from optical stellar spectroscopy.

Like our Milky Way, other spirals also rotate considerably faster in their outer regions than one would expect from Kepler's law and the distribution of visible matter (see Fig. 3.15).

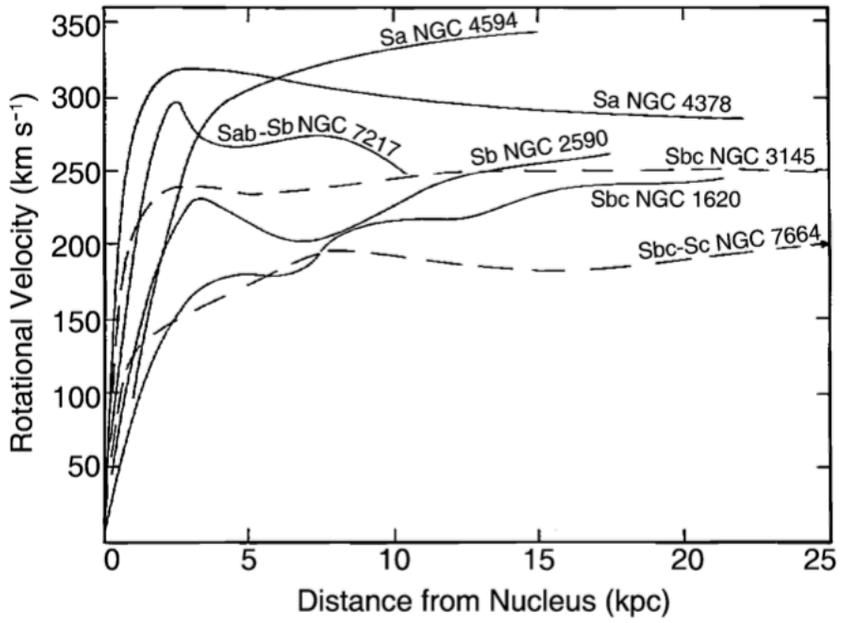

Fig. 3.15. Examples of rotation curves of spiral galaxies. They are all flat in the outer region and do not behave as expected from Kepler's law if the galaxy consisted only of luminous matter. Also striking is the fact that the amplitude of the rotation curve is higher for early types than for late types.

The rotation curves of spirals do not decrease for $R \geq h_r$, as one would expect from the light distribution, but are basically flat. We therefore conclude that spirals are surrounded by a halo of dark matter. The density distribution of this dark halo can be derived from the rotation curves.

Indeed, the density distribution of the dark matter can be derived from the rotation curves. The force balance between gravitation and centrifugal acceleration yields the Kepler rotation law,

$$v^2(R) = GM(R)/R\,,$$

from which one directly obtains the mass $M(R)$ within a radius R. The rotation curve expected from the visible matter distribution is[4]

$$v^2_{\rm lum}(R) = GM_{\rm lum}(R)/R\,.$$

$M_{\rm lum}(R)$ can be determined by assuming a constant, plausible value for the mass-to-light ratio of the luminous matter. This value is obtained either from the spectral light distribution of the stars, together with knowledge of the properties of stellar populations, or by fitting the innermost part of the rotation curve (where the mass contribution of dark matter can presumably be neglected), assuming that M/L is independent of radius for the stellar population. From this estimate of the mass-to-light ratio, the discrepancy between $v^2_{\rm lum}$ and v^2 yields the distribution of the dark matter, $v^2_{\rm dark} = v^2 - v^2_{\rm lum} = GM_{\rm dark}/R$, or

$$\boxed{M_{\rm dark}(R) = \frac{R}{G}\left[v^2(R) - v^2_{\rm lum}(R)\right]}\,. \qquad (3.12)$$

An example of this decomposition of the mass contributions is shown in Fig. 3.16.

The corresponding density profiles of the dark matter halos seem to be flat in the inner region, and decreasing as R^{-2} at large radii. It is remarkable that $\rho \propto R^{-2}$ implies a mass profile $M \propto R$, i.e., the mass of the halo increases linearly with the radius for large R. As long as the extent of the halo is undetermined the total mass of a galaxy will be unknown. Since the observed rotation curves are flat out to the largest radius for which 21-cm emission can still be observed, a lower limit for the radius of the dark halo can be obtained, $R_{\rm halo} \gtrsim 30h^{-1}$ kpc.

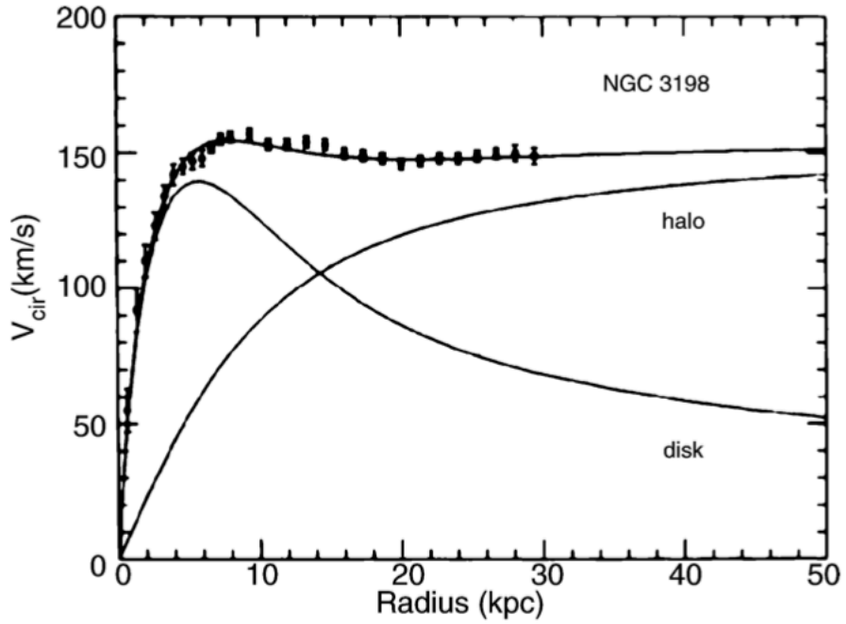

Fig. 3.16. The flat rotation curves of spiral galaxies cannot be explained by visible matter alone. The example of NGC 3198 demonstrates the rotation curve which would be expected from the visible matter alone (curve labeled "disk"). To explain the observed rotation curve, a dark matter component has to be present (curve labeled "halo"). However, the decomposition into disk and halo mass is not unambiguous because for it to be so it would be necessary to know the mass-to-light ratio of the disk. In the case considered here, a "maximum disk" was assumed, i.e., it was assumed that the innermost part of the rotation curve is produced solely by the visible matter in the disk

3.4 Scaling Relations

The kinematic properties of spirals and ellipticals are closely related to their luminosity. As we shall discuss below, spirals follow the *Tully–Fisher relation* (Sect. 3.4.1), whereas elliptical galaxies obey the *Faber–Jackson relation* (Sect. 3.4.2) and are located in the *fundamental plane* (Sect. 3.4.3). These scaling relations are a very important tool for distance estimations, as will be discussed in Sect. 3.6. Furthermore, these scaling relations express relations between galaxy properties which any successful model of galaxy evolution must be able to explain. Here we will describe these scaling relations and discuss their physical origin.

3.4.1 The Tully–Fisher Relation

Using 21-cm observations of spiral galaxies, in 1977 R. Brent Tully and J. Richard Fisher found that the maximum rotation velocity of spirals is closely related to their luminosity, following the relation

$$\boxed{L \propto v_{\rm max}^{\alpha}}\,, \qquad (3.14)$$

where the slope of the Tully–Fisher relation is about $\alpha \sim 4$. The larger the wavelength of the filter in which the luminosity is measured, the smaller the dispersion of the Tully–Fisher relation (see Fig. 3.19). This is to be expected because radiation at larger wavelengths is less affected by dust absorption and by the current star-formation rate, which may vary to some extent between individual spirals. Furthermore, it is found that the value of α increases with the wavelength of the filter; the Tully–Fisher relation is steeper in the red. The dispersion of galaxies around the relation (3.14) in the near infrared (e.g., in the H-band) is about 10%.

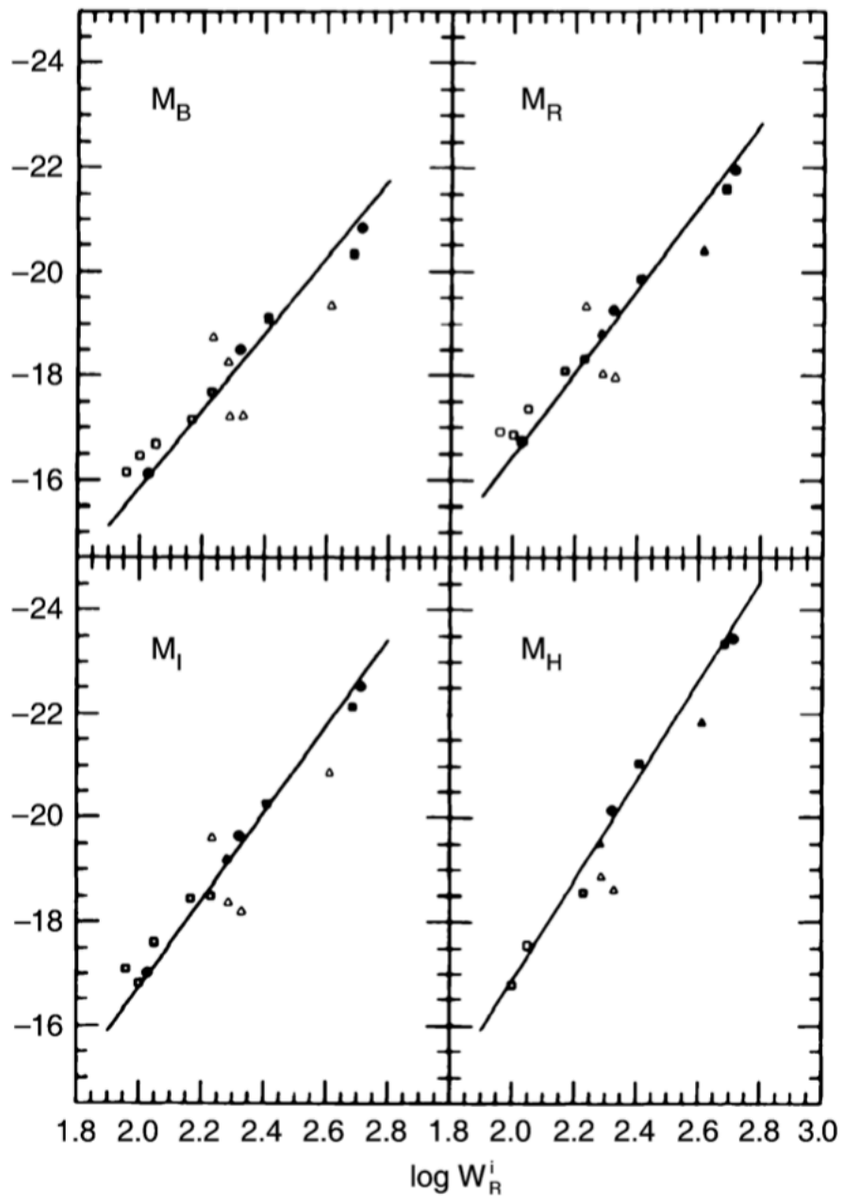

Fig. 3.19. The Tully–Fisher relation for galaxies in the Local Group (dots), in the Sculptor group (triangles), and in the M81 group (squares). The absolute magnitude is plotted as a function of the width of the 21-cm profile which indicates the maximum rotation velocity (see Fig. 3.20). Filled symbols represent galaxies for which independent distance estimates were obtained, either from RR Lyrae stars, Cepheids, or planetary nebulae. For galaxies represented by open symbols, the average distance of the respective group is used. The solid line is a fit to similar data for the Ursa-Major cluster, together with data of those galaxies for which individual distance estimates are available (filled symbols). The larger dispersion around the mean relation for the Sculptor group galaxies is due to the group's extent along the line-of-sight

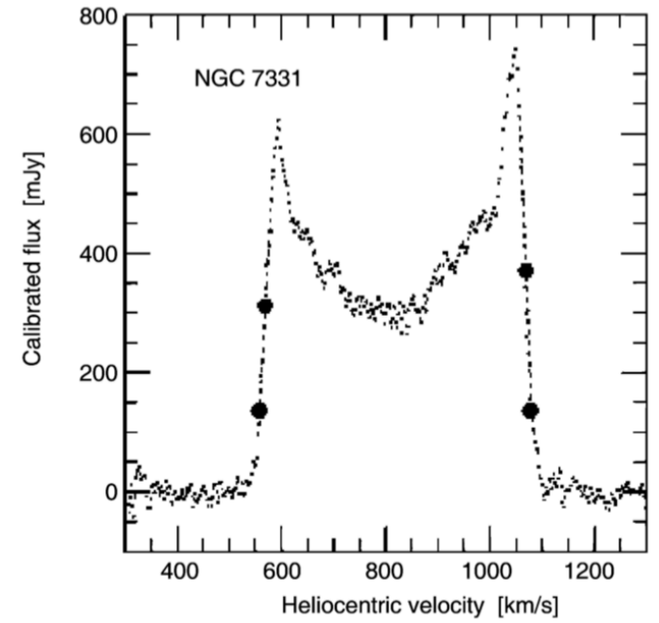

Fig. 3.20. 21 cm profile of the galaxy NGC 7331. The bold dots indicate 20% and 50% of the maximum flux; these are of relevance for the determination of the line width from which the rotational velocity is derived

Because of this close correlation, the luminosity of spirals can be estimated quite precisely by measuring the rotational velocity. The determination of the (maximum) rotational velocity is independent of the galaxy's distance. By comparing the luminosity, as determined from the Tully–Fisher relation, with the measured flux one can then estimate the distance of the galaxy – without utilizing the Hubble relation!

The measurement of $v_{\rm max}$ is obtained either from a spatially resolved rotation curve, by measuring $v_{\rm rot}(\theta)$, which is possible for relatively nearby galaxies, or by observing an integrated spectrum of the 21-cm line of HI that has a Doppler width corresponding to about $2v_{\rm max}$ (see Fig. 3.20). The Tully–Fisher relation shown in Fig. 3.19 was determined by measuring the width of the 21-cm line.

Explaining the Tully–Fisher Relation. The shapes of the rotation curves of spirals are very similar to each other, in particular with regard to their flat behavior in the outer part. The flat rotation curve implies

$$M = \frac{v_{\max}^2 R}{G} , \tag{3.15}$$

where the distance R from the center of the galaxy refers to the flat part of the rotation curve. The exact value is not important, though, if only $v(R) \approx$ const. By re-writing (3.15),

$$L = \left(\frac{M}{L}\right)^{-1} \frac{v_{\max}^2 R}{G} , \tag{3.16}$$

and replacing R by the mean surface brightness $\langle I \rangle = L/R^2$, we obtain

$$L = \left(\frac{M}{L}\right)^{-2} \left(\frac{1}{G^2 \langle I \rangle}\right) v_{\max}^4 . \tag{3.17}$$

This is the Tully–Fisher relation *if* M/L and $\langle I \rangle$ are the same for all spirals. The latter is in fact suggested by Freeman's law (Sect. 3.3.2). Since the shapes of rotation curves for spirals seem to be very similar, the radial dependence of the ratio of luminous to dark matter may also be quite similar among spirals. Furthermore, since the red or infrared mass-to-light ratios of a stellar population do not depend strongly on its age, the constancy of M/L could also be valid if dark matter is included.

Although the line of argument presented above is far from a proper derivation of the Tully–Fisher-relation, it nevertheless makes the existence of such a scaling relation plausible.

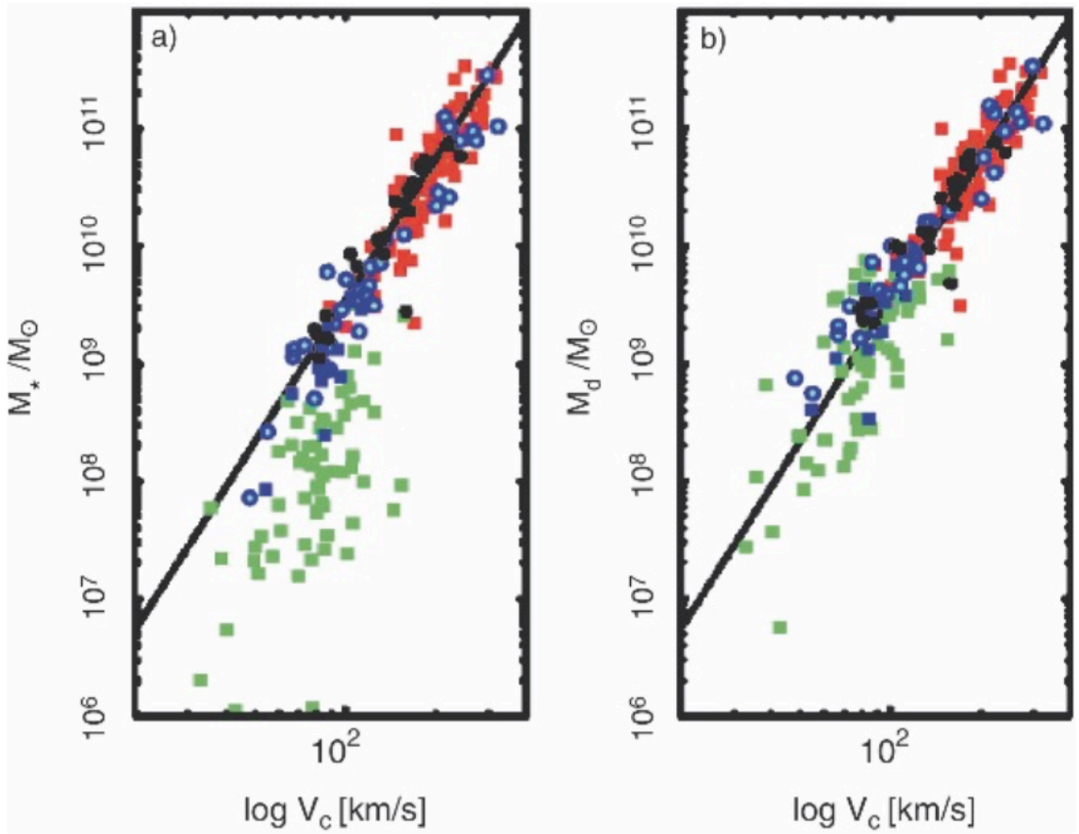

Fig. 3.21. Left panel: the mass contained in stars as a function of the rotational velocity V_c for spirals. This stellar mass is computed from the luminosity by multiplying it with a suitable stellar mass-to-light ratio which depends on the chosen filter and which can be calculated from stellar population models. This is the "classical" Tully–Fisher relation. Squares and circles denote galaxies for which V_c was determined from the 21-cm line width or from a spatially resolved rotation curve, respectively. The colors of the symbols indicate the filter band in which the luminosity was measured: H (red), K′ (black), I (green), B (blue). Right panel: instead of the stellar mass, here the sum of the stellar and gaseous mass is plotted. The gas mass was derived from the flux in the 21-cm line, $M_{\rm gas} = 1.4 M_{\rm HI}$, corrected for helium and metals. Molecular gas has no significant contribution to the baryonic mass. The line in both plots is the Tully–Fisher relation with a slope of $\alpha = 4$

3.4.2 The Faber–Jackson Relation

A relation for elliptical galaxies, analogous to the Tully–Fisher relation, was found by Sandra Faber and Roger Jackson. They discovered that the velocity dispersion in the center of ellipticals, σ_0, scales with luminosity (see Fig. 3.22),

$$\boxed{L \propto \sigma_0^4} \,,$$

or

$$\boxed{\log(\sigma_0) = -0.1 M_B + \text{const}} \,. \tag{3.20}$$

"Deriving" the Faber–Jackson scaling relation is possible under the same assumptions as the Tully–Fisher relation. However, the dispersion of ellipticals about this relation is larger than that of spirals about the Tully–Fisher relation.

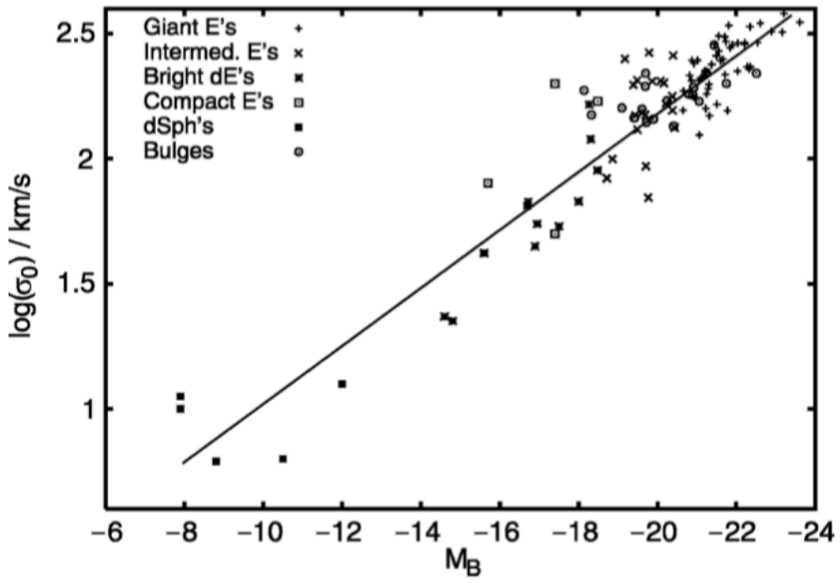

Fig. 3.22. The Faber–Jackson relation expresses a relation between the velocity dispersion and the luminosity of elliptical galaxies. It can be derived from the virial theorem

3.4.3 The Fundamental Plane

The Tully–Fisher and Faber–Jackson relations specify a connection between the luminosity and a kinematic property of galaxies. As we discussed previously, various relations exist between the parameters of elliptical galaxies. Thus one might wonder whether a relation exists between observables of elliptical galaxies for which the dispersion is smaller than that of the Faber–Jackson relation. Such a relation was indeed found and is known as the *fundamental plane*.

To explain this relation, we will consider the various relations between the parameters of ellipticals. In Sect. 3.2.2 we saw that the effective radius of normal ellipticals is related to the luminosity (see Fig. 3.7). This implies a relation between the surface brightness and the effective radius,

$$\boxed{R_\mathrm{e} \propto \langle I \rangle_\mathrm{e}^{-0.83}}\,, \tag{3.21}$$

where $\langle I \rangle_\mathrm{e}$ is the average surface brightness within the effective radius, so that

$$\boxed{L = 2\pi R_\mathrm{e}^2 \langle I \rangle_\mathrm{e}}\,. \tag{3.22}$$

From this, a relation between the luminosity and $\langle I \rangle_\mathrm{e}$ results,

$$L \propto R_\mathrm{e}^2 \langle I \rangle_\mathrm{e} \propto \langle I \rangle_\mathrm{e}^{-0.66}$$

or

$$\boxed{\langle I \rangle_\mathrm{e} \propto L^{-1.5}}\,. \tag{3.23}$$

Hence, more luminous ellipticals have smaller surface brightnesses, as is also shown in Fig. 3.7. By means of the Faber–Jackson relation, L is related to σ_0, the central velocity dispersion, and therefore, σ_0, $\langle I \rangle_\mathrm{e}$, and R_e are related to each other. The distribution of elliptical galaxies in the three-dimensional parameter space (R_e, $\langle I \rangle_\mathrm{e}$, σ_0) is located close to a plane defined by

$$\boxed{R_\mathrm{e} \propto \sigma_0^{1.4} \langle I \rangle_\mathrm{e}^{-0.85}}\,. \tag{3.24}$$

Writing this relation in logarithmic form, we obtain

$$\boxed{\log R_\mathrm{e} = 0.34 \langle \mu \rangle_\mathrm{e} + 1.4 \log \sigma_0 + \mathrm{const}}\,, \tag{3.25}$$

where $\langle \mu \rangle_\mathrm{e}$ is the average surface brightness within R_e, measured in mag/arcsec^2. Equation (3.25) defines a plane in this three-dimensional parameter space that is known as the *fundamental plane* (*FP*). Different projections of the fundamental plane are displayed in Fig. 3.23.

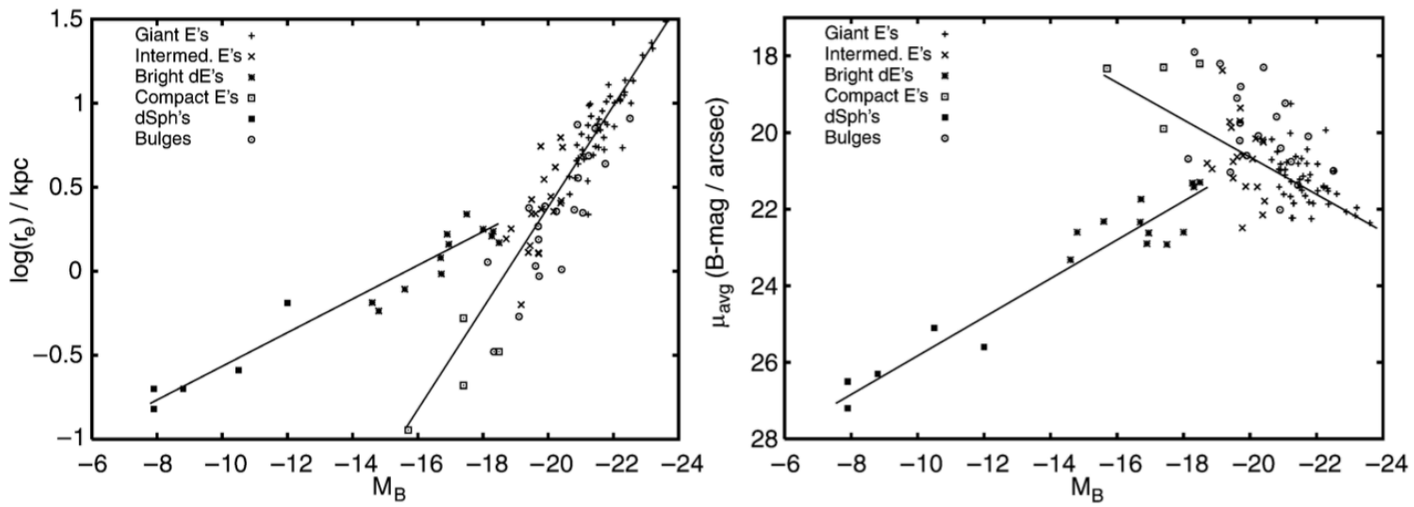

Fig. 3.7. Left panel: effective radius R_e versus absolute magnitude M_B; the correlation for normal ellipticals is different from that of dwarfs. Right panel: average surface brightness μ_ave versus M_B; for normal ellipticals, the surface brightness decreases with increasing luminosity while for dwarfs it increases

Projections of the Fundamental Plane

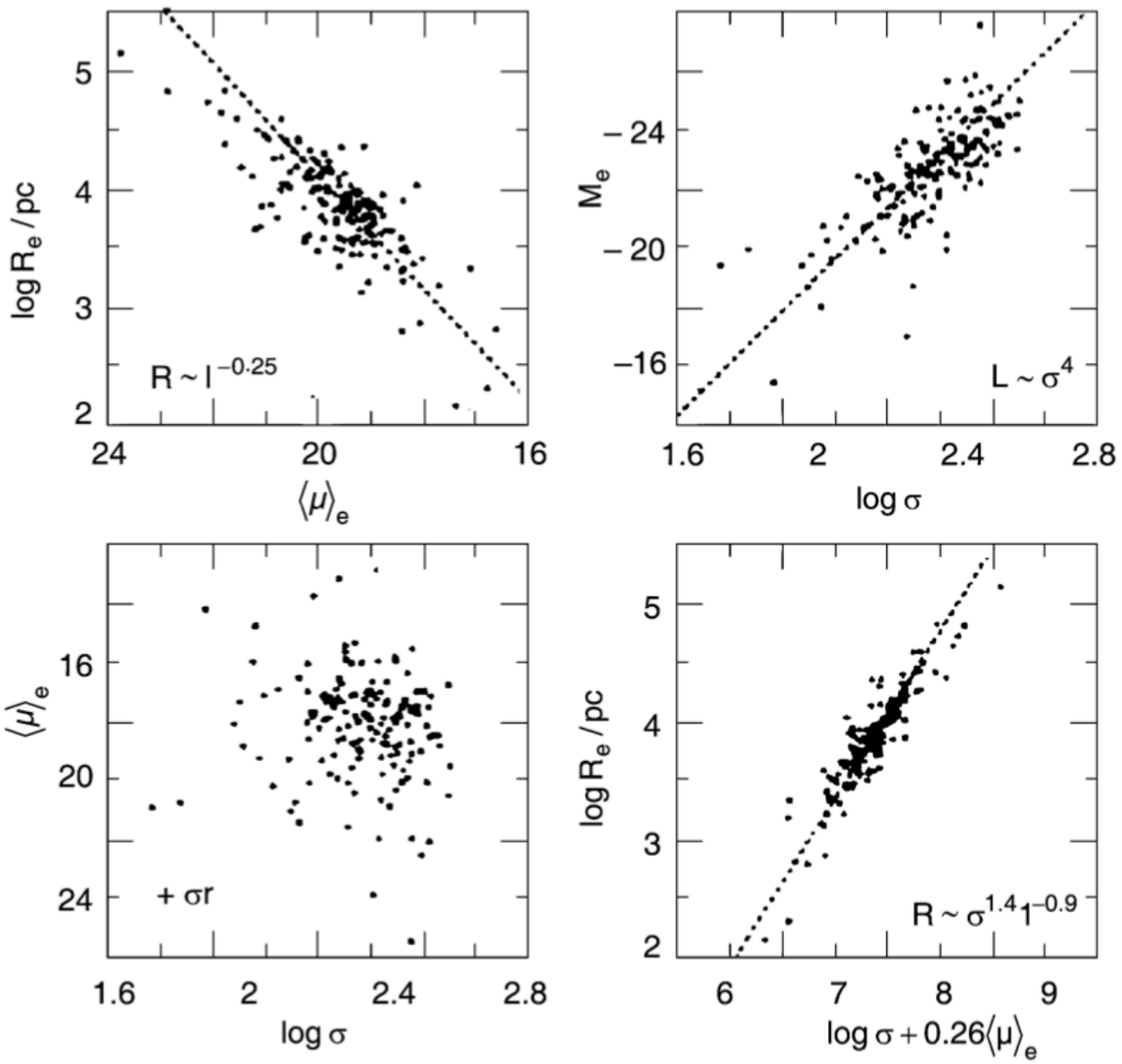

$$\log R_e = 0.34\,\langle\mu\rangle_e + 1.4\log\sigma_0 + \text{const}$$

Fig. 3.23. Projections of the fundamental plane onto different two-parameter planes. Upper left: the relation between radius and mean surface brightness within the effective radius. Upper right: Faber–Jackson relation. Lower left: the relation between mean surface brightness and velocity dispersion shows the fundamental plane viewed from above. Lower right: the fundamental plane viewed from the side – the linear relation between radius and a combination of surface brightness and velocity dispersion

The Fundamental Plane

How can this be Explained? The mass within R_e can be derived from the virial theorem, $M \propto \sigma_0^2 R_e$. Combining this with (3.22) yields

$$R_e \propto \frac{L}{M} \frac{\sigma_0^2}{\langle I \rangle_e} , \qquad (3.26)$$

which agrees with the FP in the form of (3.24) if

$$\frac{L}{M} \frac{\sigma_0^2}{\langle I \rangle_e} \propto \frac{\sigma_0^{1.4}}{\langle I \rangle_e^{0.85}} ,$$

or

$$\frac{M}{L} \propto \frac{\sigma_0^{0.6}}{\langle I \rangle_e^{0.15}} \propto \frac{M^{0.3}}{R_e^{0.3}} \frac{R_e^{0.3}}{L^{0.15}} .$$

Hence, the FP follows from the virial theorem provided

$$\left(\frac{M}{L}\right) \propto M^{0.2} \qquad \text{or}$$

$$\left(\frac{M}{L}\right) \propto L^{0.25} , \qquad \text{respectively} , \qquad (3.27)$$

i.e., if the mass-to-light ratio of galaxies increases slightly with mass. Like the Tully–Fisher relation, the fundamental plane is an important tool for distance estimations. It will be discussed more thoroughly later.

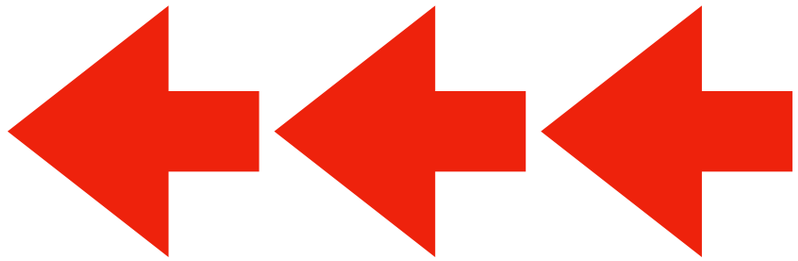

3.4.4 The D_n–σ Relation

Another scaling relation for ellipticals which is of substantial importance in practical applications is the D_n–σ relation. D_n is defined as that diameter of an ellipse within which the average surface brightness I_n corresponds to a value of 20.75 mag/arcsec^2 in the B-band. If we now assume that all ellipticals have a self-similar brightness profile, $I(R) = I_\mathrm{e}\, f(R/R_\mathrm{e})$, with $f(1) = 1$, then the luminosity within D_n can be written as

$$I_n \left(\frac{D_n}{2}\right)^2 \pi = 2\pi I_\mathrm{e} \int_0^{D_n/2} \mathrm{d}R\; R\; f(R/R_\mathrm{e})$$

$$= 2\pi I_\mathrm{e} R_\mathrm{e}^2 \int_0^{D_n/(2R_\mathrm{e})} \mathrm{d}x\; x\; f(x)\;.$$

For a de Vaucouleurs profile we have approximately $f(x) \propto x^{-1.2}$ in the relevant range of radius. Computing the integral with this expression, we obtain

$$D_n \propto R_\mathrm{e}\, I_\mathrm{e}^{0.8}\;. \tag{3.28}$$

Replacing R_e by the fundamental plane (3.24) then results in

$$D_n \propto \sigma_0^{1.4}\; \langle I\rangle_\mathrm{e}^{-0.85}\; I_\mathrm{e}^{0.8}\;.$$

Since $\langle I\rangle_\mathrm{e} \propto I_\mathrm{e}$ due to the assumed self-similar brightness profile, we finally find

$$\boxed{D_n \propto \sigma_0^{1.4}\; I_\mathrm{e}^{0.05}}\;. \tag{3.29}$$

This implies that D_n is nearly independent of I_e and only depends on σ_0. The D_n–σ relation (3.29) describes the properties of ellipticals considerably better than the Faber–Jackson relation and, in contrast to the fundamental plane, it is a relation between only two observables. Empirically, we find that ellipticals follow the normalized D_n–σ relation

$$\frac{D_n}{\mathrm{kpc}} = 2.05 \left(\frac{\sigma_0}{100\,\mathrm{km/s}}\right)^{1.33}\;, \tag{3.30}$$

and they scatter around this relation with a relative width of about 15%.